doi:10.1038/nature12775

Supplementary Figure 1. Sequence alignment of Na_VAb, Ca_VAb, human Na_V, and human Ca_V Channels. Alignment of the selectivity filter sequence of Na_VAb, Ca_VAb, and the four domains from three human Na_V and three human Ca_V channels. Two highly conserved residues that maintain the structural configuration of the filter are highlighted in green. Negatively charged and polar residues at positions corresponding to E177, S178, and M181 in Na_VAb are colored in yellow.

	selectivity filter
Na_VAb	FQVMTLESWSMG
Ca_VAb	FQVMTLDDWSDG
$hCa_V1.2I$	FQCITMEGWTDV
$hCa_V1.2II$	FQILTGEDWNSV
$hCa_V1.2III$	FTVSTFEGWPEL
$hCa_V1.2IV$	FRCATGEAWQDI
$hCa_V2.1I$	FQCITMEGWTDL
$hCa_V2.1II$	FQILTGEDWNEV
$hCa_V2.1III$	FTVSTGEGWPQV
$hCa_V2.1IV$	FRSATGEAWHNI
$hCa_V3.2I$	FQVITLEGWVDI
$hCa_V3.2II$	FQILTQEDWNVV
$hCa_V3.2III$	FVLSSKDGWVNI
$hCa_V3.2IV$	FRVSTGDNWNGI
$hNa_V1.1I$	FRLMTQDFWENL
$hNa_V1.1II$	FRVLCGE-WIET
$hNa_V1.1III$	LQVATFKGWMDI
$hNa_V1.1IV$	FQITTSAGWDGL
$hNa_V1.4I$	FRLMTQDYWENL
$hNa_V1.4II$	FRILCGE-WIET
$hNa_V1.4III$	LQVATFKGWMDI
$hNa_V1.4IV$	FEITTSAGWDGL
$hNa_V1.7I$	FRLMTQDYWENL
$hNa_V1.7II$	FRVLCGE-WIET
$hNa_V1.7III$	LQVATFKGWTII
$hNa_V1.7IV$	FQITTSAGWDGL

Supplementary Figure 2. Reversal potentials of Ca_VAb and intermediates measured under bi-ionic conditions. Extracellular solution contained either 10 mM Ca^{2+} (blue) or 10 mM Ba^{2+} (green). **a.** ^{175}TLDDWSN^{181} mutant raw traces measured in Ca (blue traces) or Ba (green traces). Cells were held at -100 mV, and 20 ms depolarizing pulses were applied in 10 mV steps. **b.** Averaged I-V curves for the representative raw traces shown in a. E_{rev} for Ca as the permeant ion was +35 mV, while it was +7.5 mV for Ba ions. **c, d.** As in panel a,b but for ^{175}TLEDWSD^{181}. **e, f.** ^{175}TLEDWSM^{181}. **g, h,** ^{175}TLDDWSM^{181}. **i, j.** ^{175}TLDSWSM^{181}. ^{175}TLDDWSM^{181} failed to produce ionic current in these solutions even though expression was high. When EGTA was added to both intracellular and extracellular solutions, large Na currents were observed with this mutant. Errors bars are standard error of the mean.

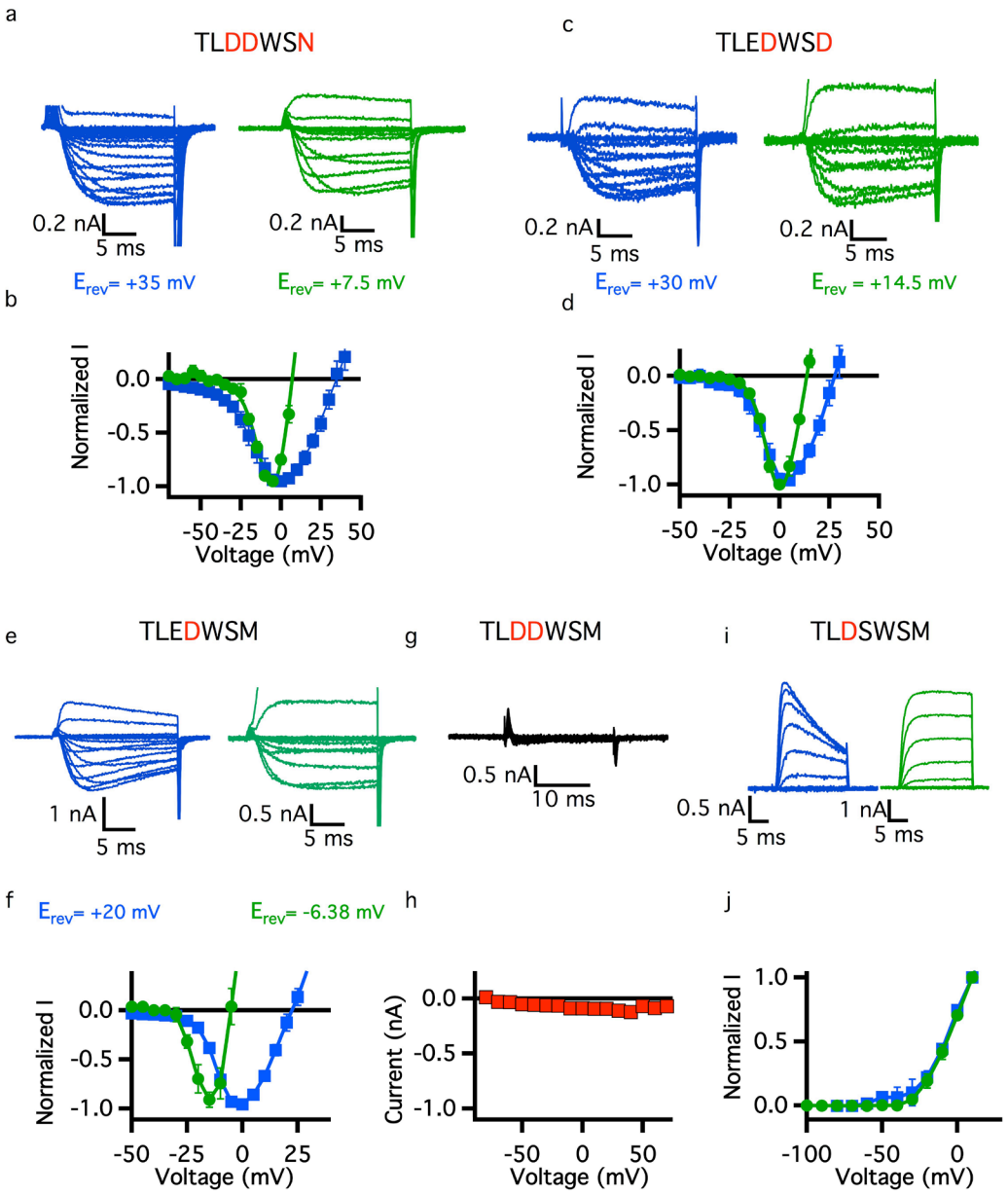

Supplementary Figure 3. Protein surface electrostatic potential of Na_VAb (^{175}TLESWSM^{181}), ^{175}TLDDWSN^{181} and Ca_VAb (^{175}TLDDWSD^{181}). The electrostatic potential on the surface of Na_VAb (^{175}TLESWSM^{181}), ^{175}TLDDWSN^{181}, and Ca_VAb (^{175}TLDDWSD^{181}) viewed from the extracellular side. Electronegative and electropositive charges are colored in red and blue, respectively.

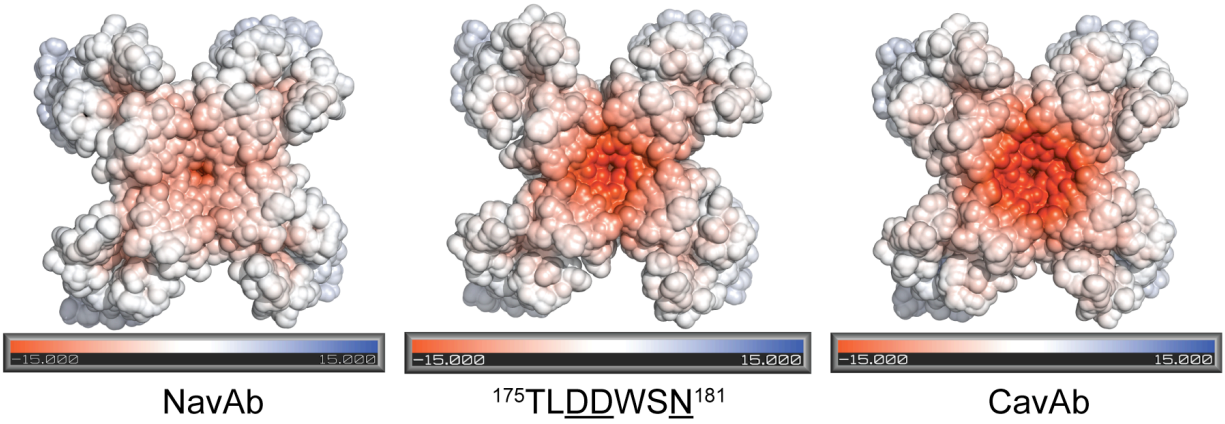

Supplementary Figure 4. Structure of the selectivity filter (residues 175-181) of ^{175}TLDDWSN^{181}. **a,b,c,d** An |Fo-Fc| simulated annealing omit map contoured at 3σ in which the selectivity filter of each molecule was omitted for map calculation.

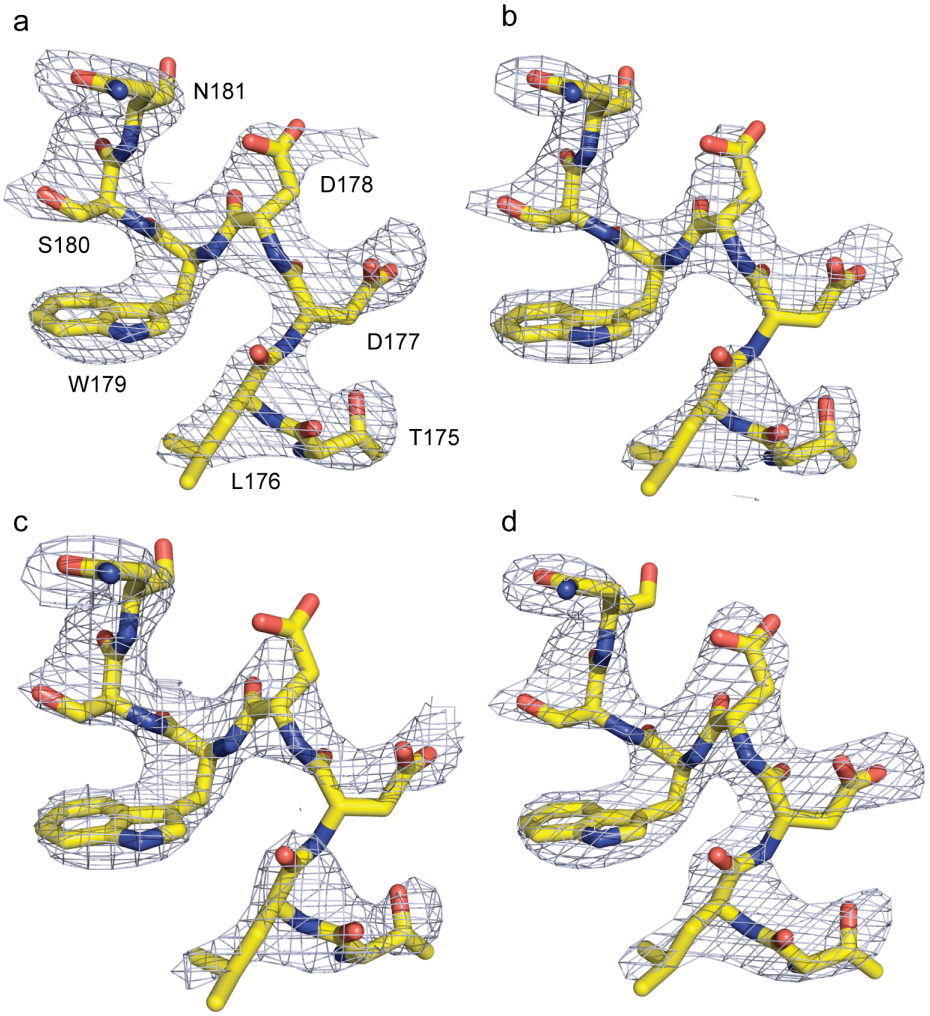

Supplementary Figure 5. Evidence for hydration shells for Ca^{2+}, Cd^{2+} and Mn^{2+} bound at the selectivity filter. The ionic radii for Ca^{2+}, Cd^{2+} and Mn^{2+} are 1.14 Å, 1.09 Å and 0.97 Å respectively. The distances between the coordinating residue and Ca^{2+}, Cd^{2+}, Mn^{2+} are in a similar range of 4-5Å. The anomalous difference Fourier maps (blue mesh) are contoured at 8σ, 34σ and 11σ for Ca^{2+}(**a**), Cd^{2+}(**b**) and Mn^{2+}(**c**) at site 2, in sizes reflecting the real atom ionic radius. The |Fo-Fc| omit maps (red mesh) are calculated without ion and water included in the model and contoured at 3σ(red mesh) for Ca^{2+}(**a**), Cd^{2+}(**b**) and Mn^{2+}(**c**) at site 2, indicating the likely hydration shell of Ca^{2+}, Cd^{2+} and Mn^{2+}. **d, e, f,** 2|Fo-Fc| maps (grey mesh), contoured at 1.3σ, 2σ and 2σ, were calculated after potential hydrated ions (Ca^{2+}-$8H_2O$, Cd^{2+}-$6H_2O$ and Mn^{2+} -$6H_2O$) were included in the model and refined. All three datasets are collected at 1.75 Å wavelength, with crystals ^{175}TLDDWSN^{181} soaked with10 mM Ca^{2+} (**a** and **d**), ^{175}TLDDWSD^{181} soaked with 100 mM Cd^{2+}(**b** and **e**), and ^{175}TLDDWSD^{181}soaked with 100 mM Mn^{2+} (**c** and **f**). To better define the position of H_2O in the selectivity filter, one 2.75 Å dataset was collected with the ^{175}TLDDWSN^{181} crystals soaked with cryo-protectant solutions containing 15 mM Ca^{2+}. **g**, Coordination of the Ca^{2+}-nH2O complex at the three binding sites. The distance between oxygen atoms or oxygen atom and Ca^{2+} is shown in Å. **h**, An |Fo-Fc| simulated annealing omit map contoured at 2.5σ for site 1 and 2 was calculated from the model in which the Ca^{2+}-nH_2O complex was omitted. **i**, An |Fo-Fc| simulated annealing omit map contoured at 2.5σ for calcium binding Site 3 (Top view).

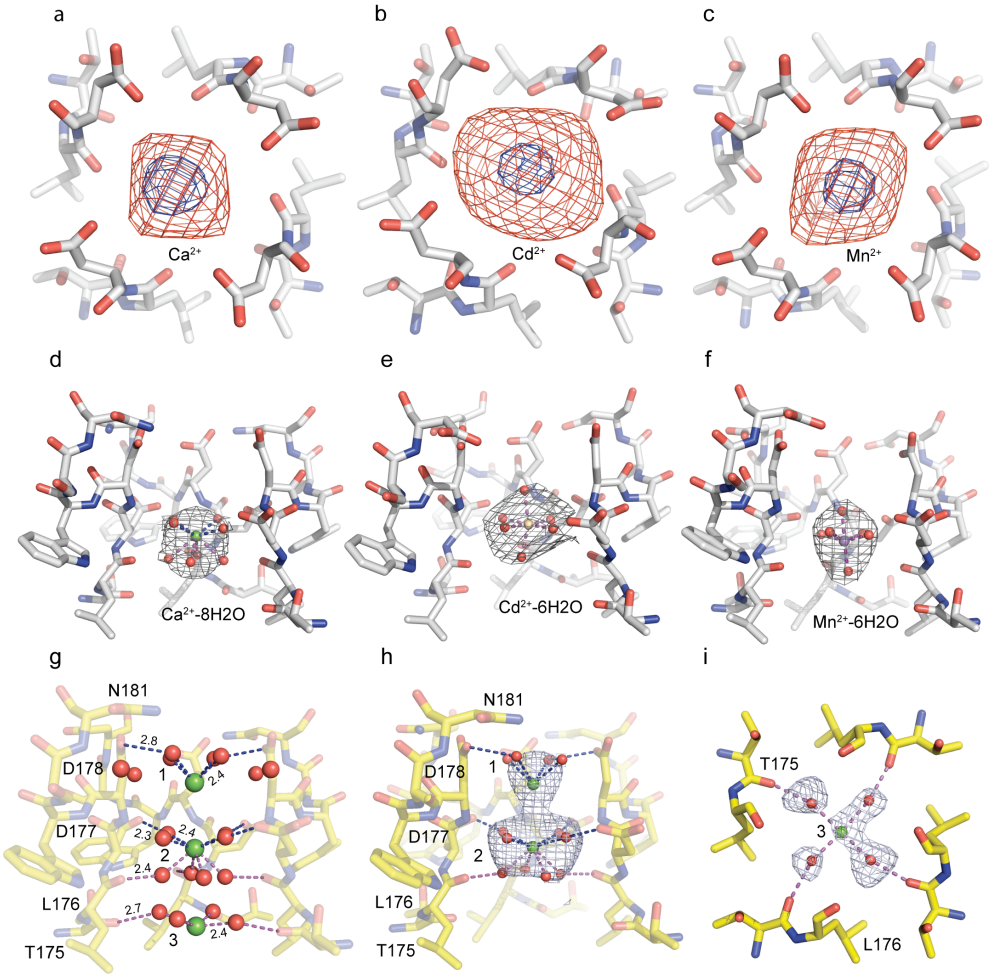

Supplementary Figure 6. Ca^{2+} binding at the selectivity filter sites of Na_VAb, Ca_VAb, and their derivatives. **a, b,** Side view of the selectivity filter (sticks) of ^{175}TLEDWSM^{181} and ^{175}TLESWSM^{181} with the anomalous difference Fourier map density at Site 1 and 2 (blue mesh, contoured at 3σ) calculated with diffraction data of crystals collected at 1.75 Å wavelength. **c,d,** Top view of the selectivity filter (sticks) at site 2 for ^{175}TLDDWSD^{181} and ^{175}TLEDWSD^{181}with the anomalous difference Fourier map density at Site 2 (blue mesh, contoured at 5σ) calculated with diffraction data of crystals collected at 1.75 Å wavelength.

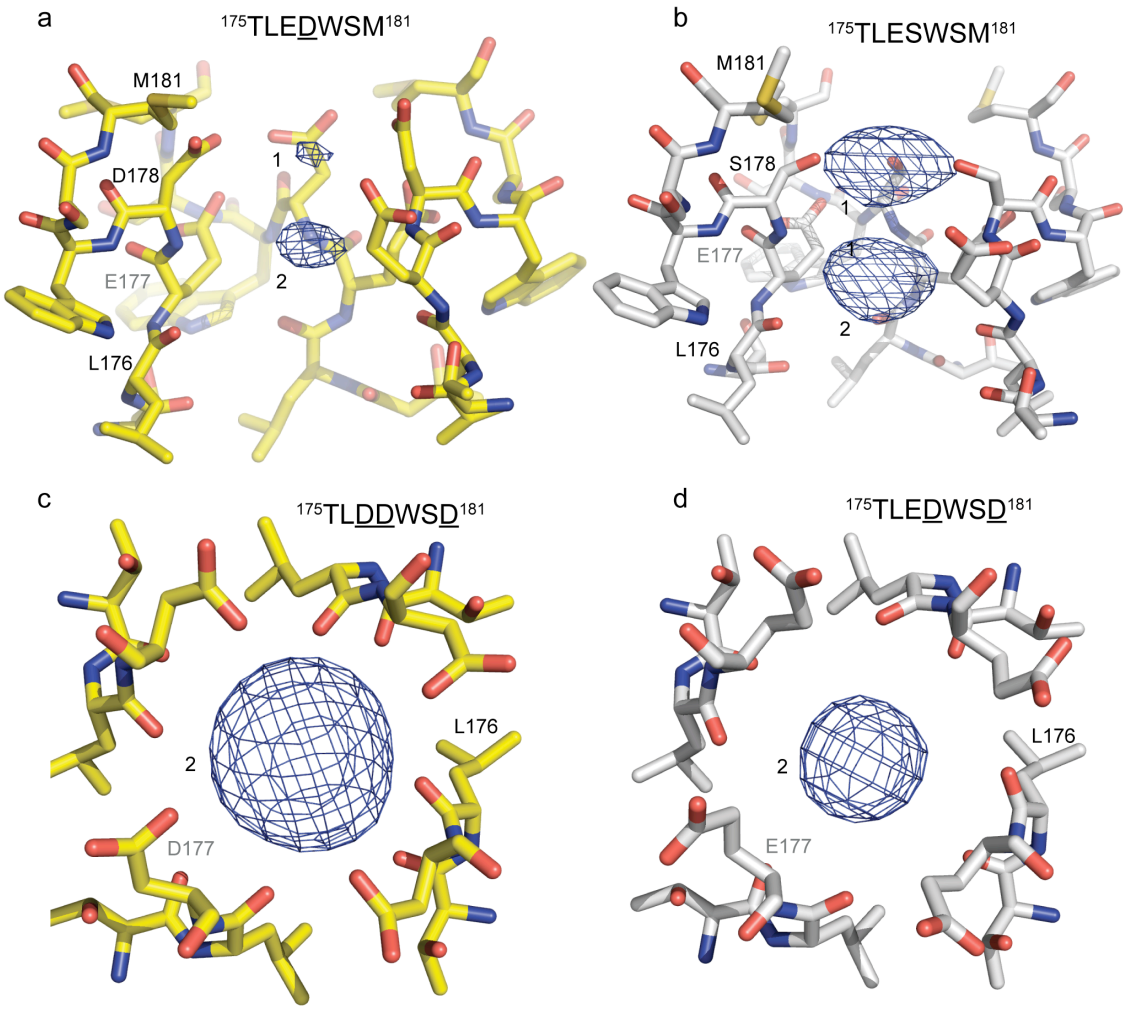

Supplementary Figure 7. Structural comparison of the selectivity filter of ^{175}TLEDWSD^{181} and ^{175}TLDDWSD^{181}. **a,** Superposition of ^{175}TLDDWSD^{181} (yellow) and ^{175}TLEDWSD^{181} (grey) at Site 2 (Site$_{HFS}$/Site$_{CEN}$) viewed from the side. The distance between the carboxyl oxygen of E177 to the main chain nitrogen of S180 and D181 is around 2.9 Å and 3.3 Å, respectively (magenta dash line). **b**, Superposition of ^{175}TLDDWSD^{181} (yellow) and ^{175}TLEDWSD^{181} (grey) at Site 2 (Site$_{HFS}$/Site$_{CEN}$) viewed from the top. **c**, An |Fo-Fc| simulated annealing omit map contoured at 3σ with residue E177, D178, S180, and D181 of ^{175}**TLEDWSD**^{181} omitted for map calculation. **d**, LIGPLOT representation of residues E177 and D178 in one subunit (purple) of ^{175}**TLEDWSD**^{181} interacting with residues S180 and D181 of the adjacent subunit (orange).

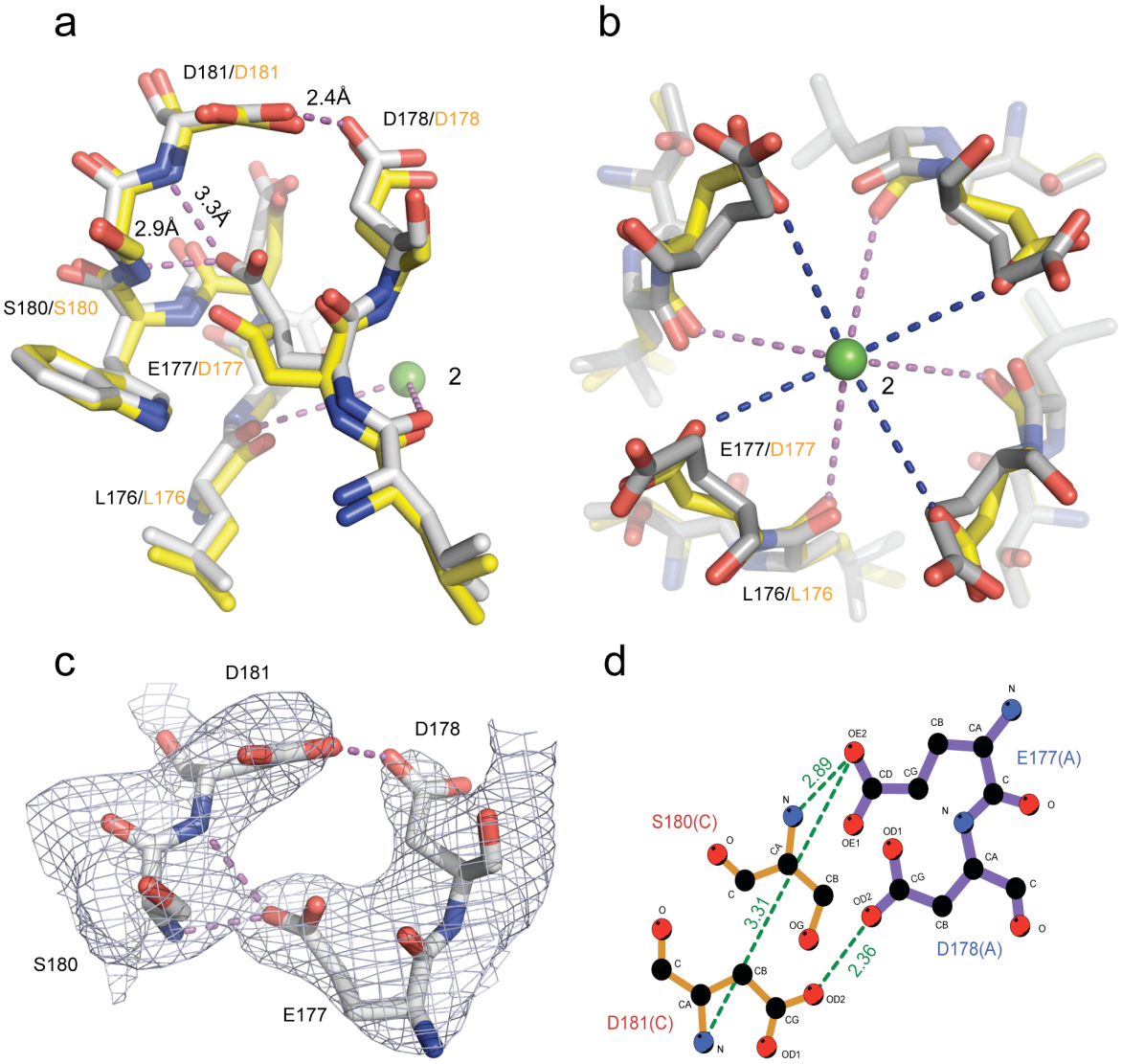

Supplementary Figure 8. Evidence for hydrogen bonds and carboxyl-carboxylate pairs at the selectivity filter entryway. **a,b,** Top view of an |Fo-Fc| simulated annealing omit map contoured at 3σ for residues 177 and 181 of ^{175}TLDDWSN^{181} and ^{175}TLDDWSD^{181}. **c**, An |Fo-Fc| simulated annealing omit map contoured at 2.5σ for E177 and D178 of ^{175}TLEDWSM^{181}. **d, e**, LIGPLOT diagrams for residues from 177 and 181 in the selectivity filter of ^{175}TLDDWSN^{181} and ^{175}TLDDWSD^{181}. **f**, LIGPLOT representation of residue 177 and 178 in one subunit of ^{175}TLEDWSM^{181} interacting their nearby residues.

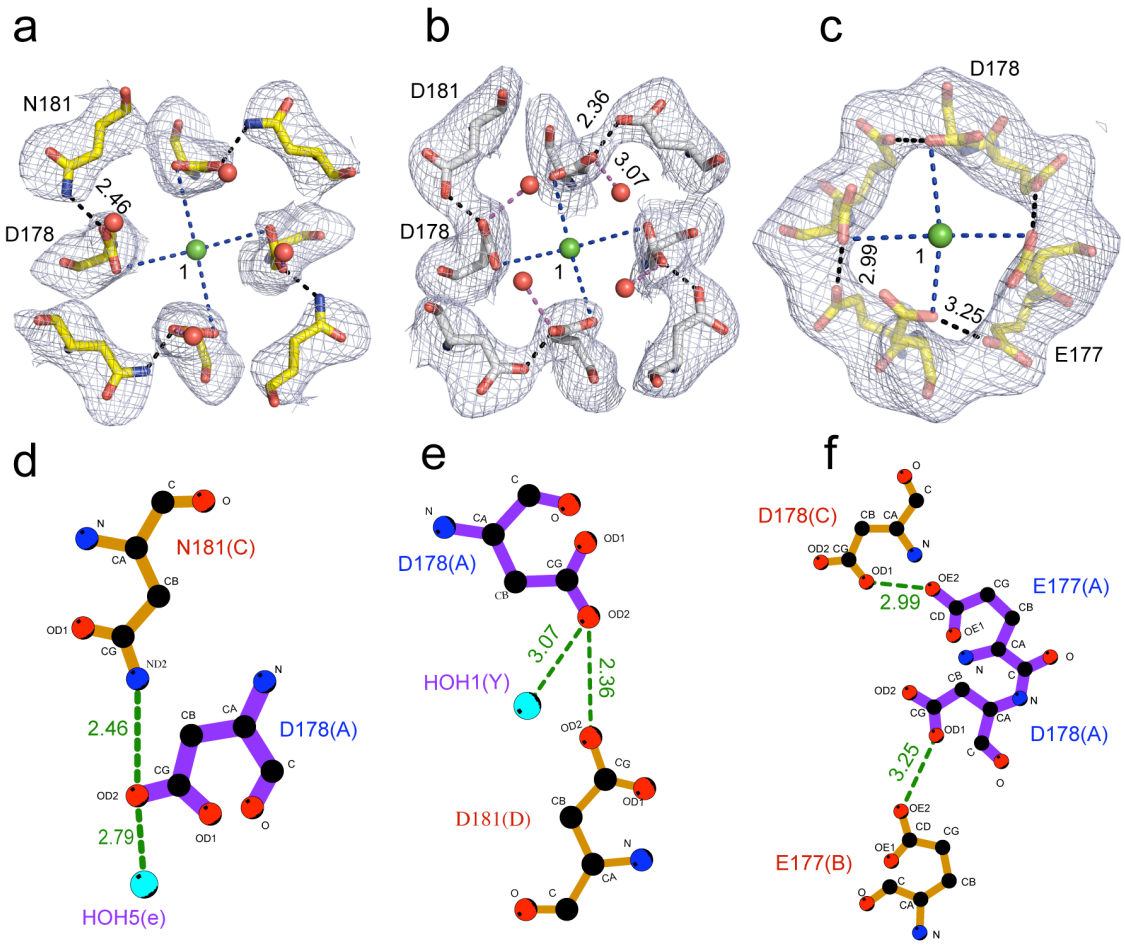

Supplementary Figure 9. Ca^{2+} binding at the selectivity filter sites of ^{175}TLDDWSN^{181}. Side view of the selectivity filter (sticks) of ^{175}TLDDWSN^{181} with the anomalous difference Fourier map density at Site 1 and 2 (blue mesh, contoured at 5σ) calculated with diffraction data of crystals collected at 1.75 Å wavelength. Before data collection, the crystals were soaked with cryo-protectant solutions containing 0.5 mM (a), 2.5 mM (b), 5mM(c), 10mM(d) and 15 mM (c) Ca^{2+}.

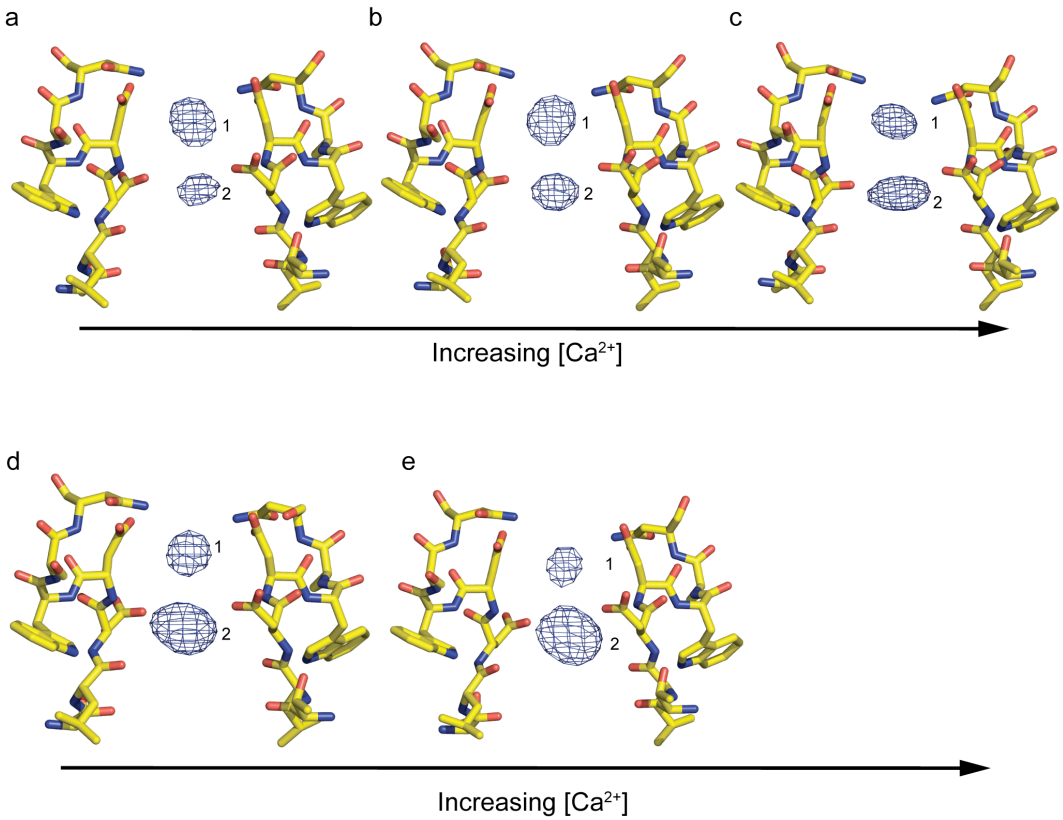

Supplementary Table 1. Data collection, phasing and refinement statistics.

	TLDDWSN+ Ca^{2+}						TLESWSM+Ca^{2+}
	0.5mM	2.5mM	5mM	10mM	15mM	15mM	15mM
Data collection							
Space group	C121	C121	C121	C121	C121	C121	C121
Cell dimensions							
a, *b*, *c* (Å)	177.7	177.3	176.6	177.5	177.5	177.8	229.2
	177.8	177.7	177.7	177.9	177.5	177.8	124.9
	131.1	130.9	130.6	130.9	131.0	131.1	124.8
α, β, γ (°)	90	90	90	90	90	90	90
	132.7	132.6	132.5	132.54	132.63	132.69	123.0
	90	90	90	90	90	90	90
Resolution (Å)	3.3	3.3	3.4	3.2	3.3	2.75	3.3
R_{sym} or R_{merge}	0.087	0.09	0.125	0.091	0.07	0.078	0.09
$I/\sigma I$	10.3 (2.2)	8.8(2.1)	7.7(2.0)	9.7/1.8	11.2/2.5	6.9/1.5	13.7(1.9)
Completeness (%)	92.7(82.3)	98.4(98.9)	90.5(93.4)	96.5(98)	93.9(84.4)	94.18(84.11)	85.83(66.87)
Redundancy	5.0 (5.0)	4.8(4.8)	5.4(5.2)	5.1(5.0)	4.8(4.8)	2.6(2.5)	2.5(2.4)
Refinement							
Resolution (Å)	30-3.3	29.9-3.3	30-3.4	30-3.2	30-3.3	40-2.75	40.7-3.3
No. reflections	45979	42440	36860	47487	42145	74174	39791
R_{work}/ R_{free}	24.1/27.1	23.9/27.3	24.0/28.4	25.4/27.7	26.0/28.0	23.1/25.5	27.6/31.5
No. atoms	7386	7386	7387	7407	7391	7889	7378
Protein	7192	7192	7192	7192	7192	7192	7188
Ligand/ion	190	190	191	193	191	659	190
Water	4	4	4	22	8	38	
B-factors							
Protein	101.7	99.2	106.5	103.4	92.0	75.3	94.0
Ligand/ion	94.8	93	98	88.0	75.0	75.2	86.3
Water	32	28.3	55.4	65.5	40.3	48.2	
R.m.s deviations							
Bond lengths (Å)	0.015	0.012	0.018	0.014	0.013	0.01	0.014
Bond angles (°)	1.55	1.54	1.74	1.58	1.57	1.43	1.67

Supplementary Table 1. Data collection, phasing and refinement statistics.

	TLEDWSM 15mM Ca^{2+}	TLEDWSD 15mM Ca^{2+}	TLDDWSM 15mM Ca^{2+}	TLDDWSD 100mM Cd^{2+}	TLDDWSD 100mM Mn^{2+}	TLDDWSD 15mM Ca^{2+}
Data collection						
Space group	C121	C121	C121	C121	C121	C121
Cell dimensions						
a, *b*, *c* (Å)	177.8	178	177.8	178.6	177.4	177.8
	177.7	178	176.7	178.6	177.5	177.7131
	131.2	131.2	131.1	130.8	130.82	
α, β, γ (°)	90	90	90	90	90	90
	132.6	132.6	132.6	132.9	132.7	132.8
	90	90	90	90	90	90
Resolution (Å)	3.2	3.3	3.3	3.3	3.2	3.4
R_{sym} or R_{merge}	0.076	0.072	0.095	0.1	0.128	0.103
$I/\sigma I$	10.5 (2.5)	10.1(2.6)	9.6(1.9)	9.9/2.3	7.2(1.7)	8.5/2.7
Completeness (%)	93.4(100)	96.4(98)	88.0(92.3)	89.2(91.6)	94.9(91.7)	96.3(98.1)
Redundancy	5.0 (4.9)	5.1(5.1)	5.6(5.3)	5.5(5.4)	5.0(5.1)	5.1(5.0)
Refinement						
Resolution (Å)	30-3.2	30-3.3	42.3-3.3	28.5-3.3	35.0-3.2	28.1-3.4
No. reflections	46122	43001	39450	40379	46686	39362
R_{work}/ R_{free}	23.7/26.3	24.2/27.9	24.9/26.7	23.5(27.2)	23.9(28.7)	27.9(31.2)
No. atoms	7391	7386	7387	7391	7387	7386
Protein	7196	7196	7192	7192	7192	7192
Ligand/ion	191	190	191	193	189	190
Water	4		4	6	6	4
B-factors						
Protein	96.8	95.6	70.8	102.5	92.30	91.60
Ligand/ion	95.0	95.3	54.6	93.4	87.60	76.80
Water	85.2		36.1	43.0	78.5	69.7
R.m.s deviations						
Bond lengths (Å)	0.013	0.014	0.015	0.014	0.013	0.015
Bond angles (°)	1.61	1.60	1.77	1.61	1.64	1.80